A One-Step and Binder-Free Method to Fabricate Hierarchical Nickel-Based Supercapacitor Electrodes with Excellent Performance

Guoge Zhang, Wenfang Li, Keyu Xie, Fei Yu, and Haitao Huang**

Research is currently being carried out in the search for alternative electrode materials to replace the expensive and toxic RuO_2-based electrode. As a typical example, nickel oxide or hydroxide has been widely studied but the results are far from satisfactory. Here, using a facile one-step anodization method, a hierarchical nickel compound (HNC) film with an interconnecting 3D nanoflake structure is obtained, providing large electrochemically active surface area and interconnecting nanoscale pore channels for ion transport. The HNC electrode demonstrates significantly improved capacitance, 70 times higher than the reported NiO-TiO_2 nanotube array electrode with similar thickness. The charge/discharge kinetics are also superior, showing only a 24% capacitance reduction when the scan rate is increased by 50 times, as compared with the typical 70% capacitance reduction for pseudocapacitor electrodes under the same conditions. HNC exhibits an extraordinary excellent cycle life; capacitance increases to 115% after 4500 test cycles. Furthermore, because HNC is in intimate contact with the current collector, it is not necessary to use conducting agents or binders, which reduces the electrode weight and facilitates the electrode preparation process. The method is low cost, facile, scalable, additive free, and is promising for fabricating supercapacitor electrode with excellent performance.

1. Introduction

Nickel compounds have attracted significant interest in different areas such as catalysts,[1] energy storage,[2–6] electrochromic devices[7] and sensors.[8] However, there are still some problems hindering the practical application of nickel compounds, such as tedious and time-consuming preparation technique or structural instability. Taking the application in supercapacitors as an example, there are mainly two types of fabrication methods for nickel-based electrodes. One is to synthesize nanoparticles by various techniques such as thermal decomposition,[9] sol-gel,[10] hydrothermal process[11] and precipitation.[12] The nanoparticles are then mixed thoroughly with binder and conducting agent. The resulting paste is pressed onto a current collector (stainless steel or nickel foam, etc.) to form an electrode. The other is to deposit nickel compounds directly on the current collector by chemical deposition,[13] sputtering[14] or electrochemical deposition.[15,16] The first type of fabrication methods is complicated and time-consuming, and the poor conductivity of binder results in reduced power performance. The second type of methods suffers from relatively weak adhesion between the nickel-based material and the current collector, leading to the loss of active material and short cycle life of supercapacitor electrode.[16] It is still challenging today to develop a synthesis method for nickel-based supercapacitor electrode with both excellent performance and high fabrication efficiency.[17]

Anodization is a fast and simple method to fabricate nanostructured oxide film, and has been used successfully on aluminum,[18] titanium,[19–22] zirconium,[23] tantalum,[24] iron[25] and niobium.[26] The anodic films demonstrate outstanding performance in versatile applications such as dye sensitized solar cells,[27–29] electrochromic devices,[30] sensors,[31] photocatalysis,[24,32,33] supercapacitors,[34,35] and biomedical applications.[23] It is straightforward to expect that anodization may also work on nickel to produce material with excellent performance and help solving the problems as mentioned above. However, since Ni is not a valve metal like Al or Ti, it is difficult to obtain anodic nanoporous nickel-based film.[36] Up to now there are very limited reports on the anodization of nickel or nickel alloy.[36,37] In ref. [36], oriented NiO-TiO_2 nanotube arrays were obatined by anodization of Ni-Ti alloy and were used as supercapacitor electrodes. However, the specific capacitance was only around 2.3 mF cm^{-2} at 500 mV s^{-1}. In ref. [37], nanoporous NiO/NiF_2 composite layers were grown by anodization of Ni in a solution containing NH_4F and H_3PO_4. The cycling stability was not so satisfactory and the electrochromic performance was reduced by 25% after 1400 cycles.

In this report, for the first time, mechanically robust hierarchical nickel compound (HNC) film was fabricated by a facile

Dr. G. Zhang, Prof. W. Li, Dr. F. Yu
School of Materials Science and Engineering
South China University of Technology
Guang Zhou, 510640, P. R. China
E-mail: ggzhang@scut.edu.cn
Dr. G. Zhang, Dr. K. Xie, Prof. H. Huang
Department of Applied Physics
The Hong Kong Polytechnic University
Hung Hom, Kowloon, Hong Kong
E-mail: aphhuang@polyu.edu.hk

DOI: 10.1002/adfm.201203418

and one-step electrochemical process. The unique structure of HNC with 3D interconnecting nanoflakes and nanoscale open channels were achieved by the fine control of anodization conditions. Due to the large surface area and the inherent active nature of nickel compound, the synthesized HNC film was evaluated as a supercapacitor electrode. Considering that HNC is grown in-situ and possesses good mechanical/electrical contact with the current collector, HNC can be used directly as an electrode without the need to add either conducting agents or binders. Such additive-free approach not only reduces the electrode weight/volume but also expedites the electrode preparation process. As a result of good electrochemical activity and highly porous morphology, HNC demonstrated significantly higher capacitance (70 times higher) than the NiO-TiO_2 nanotube arrays with similar thickness.[36] The charge/discharge kinetics was also superior for HNC. Even when the scan rate was increased to 50 times (from 10 mV s^{-1} to an ultra-fast rate of 500 mV s^{-1}), the capacitance reduction was only 24%. Such performance is remarkable as compared to the recently reported value of more than 70% capacitance reduction for pseudocapacitor electrodes under the same condition.[3,38,39] Furthermore, HNC exhibited an impressive cycle life (capacitance increases to 115% after 4500 test cycles) due to the structural stability and the resistance to material loss. Our method is simple, low cost, and additive/template free and can be easily scaled up. The work reported here provides an exciting direction to fabricate supercapacitor electrode with excellent performance.

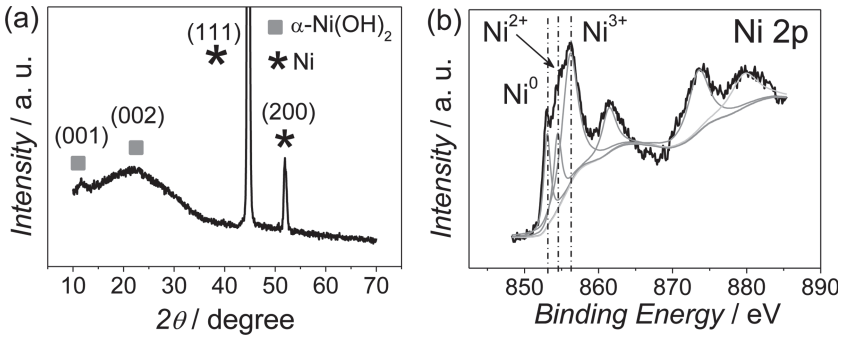

Figure 2. a) XRD and b) XPS spectrum of HNC.

2. Results and Discussion

2.1. Morphological and Structural Characterization

Figure 1 displays the scanning electron microscopy (SEM) images of anodic nickel compound. The as-prepared sample exhibited a hierarchical morphology with interconnecting nanoflakes, composing of evenly distributed nanoscale open channels. Such 3D structure with a high percentage of porosity is able to facilitate the penetration of electrolyte, providing reduced contact resistance and enhanced mass/charge transfer at the electrode/electrolyte interface. Moreover, the nanoscale thickness of nanoflakes has the advantages of shortening the diffusion distance, increasing the utilization of active material and being able to accommodate the volume changes during faradaic reaction. All the above advantages are crucial to energy storage applications where high power density and good cycle life are required. The HNC film thickness was around 400 nm as seen from Figure 1b.

Figure 2a shows the X-ray diffraction (XRD) pattern of HNC. The diffraction peaks at 44.5° and 51.9° can be indexed to (111) and (200) planes of Ni substrate beneath the anodic film (PDF # 87–0712). α-$Ni(OH)_2$ was detected at 11.5° for (001) plane and 23.3° for (002) plane (PDF # 22–0444). The broad diffraction peaks indicated that the α-$Ni(OH)_2$ had a small grain size which could contribute to the enhanced electrochemical performance.[40] There are two polymorphs of $Ni(OH)_2$, i.e., α and β phases,[41] with the first being isostructure of hydrotalcite-like compounds and the second being brucite-like. β-$Ni(OH)_2$ is characterized by perfect stacking along the *c*-axis without any intercalated species, while α-$Ni(OH)_2$ is randomly oriented and separated by intercalated water molecules or charge balancing anions (such as NO_3^-, Cl^- and SO_4^{2-}, etc.). Normally, α-$Ni(OH)_2$ exhibits better energy storage performance due to the turbostratic structure and large interlayer spacing.[42] Therefore the HNC fabricated here was expected to show good electrochemical activity.

The surface information of HNC can be found from the X-ray photoelectron spectroscopy (XPS) shown in Figure 2b. Three distinct $2p_{3/2}$ peaks were observed at 853.0, 854.4, and 856.1 eV, corresponding to the nickel oxidation states of 0, +2, and +3, respectively.[43] The detection of Ni^0 was attributed to the residual nickel in HNC. The presence of Ni^{2+} was ascribed to α-$Ni(OH)_2$. As no crystalline phase containing Ni^{3+} was determined from XRD, it is suggested that Ni^{3+} ions existed in an amorphous phase. Although α-$Ni(OH)_2$ is an attractive supercapacitor material due to the high theoretical specific capacitance, its poor conductivity is the limiting factor for high power density.[44] In HNC, the atomic ratio of Ni^0 to Ni^{2+} and Ni^{3+} was 1:1.23:3.61 as calculated from the peak areas. The existence

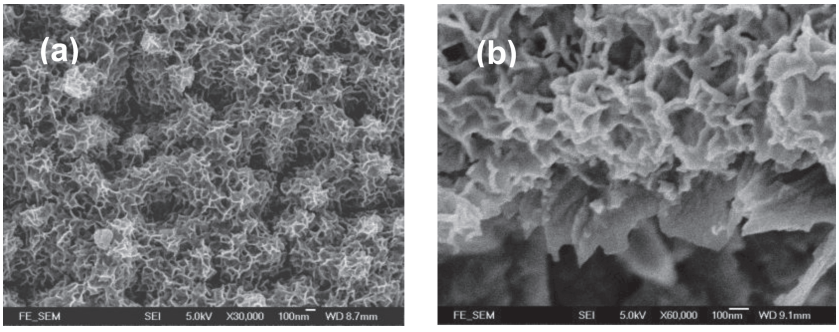

Figure 1. SEM images of the HNC at different magnifications.

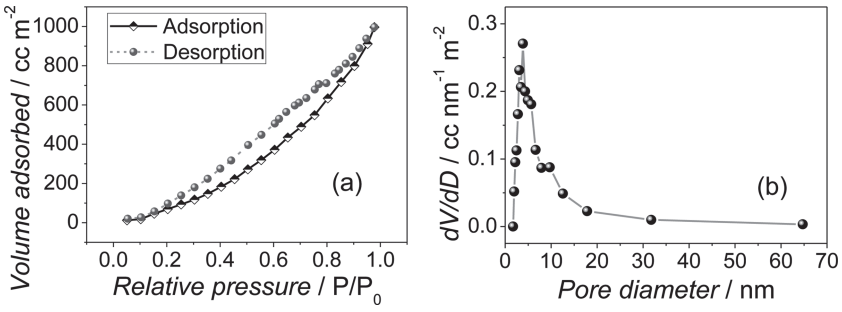

Figure 3. a) N_2 adsorption-desorption isotherm and b) pore size distribution of the HNC.

of large amounts of conductive Ni^{3+} ions and metallic Ni is beneficial to the electron conduction and contributes significantly to the rate performance which will be demonstrated below.[45] Besides the main components such as Ni and O, small quantities of S and Cl (2.07 and 0.67 at%, respectively) were also detected by XPS, which were attributed to the intercalation or adsorption of anions such as SO_4^{2-} and Cl^-.

N_2 adsorption/desorption isotherm of HNC is shown in **Figure 3**a. The hysteresis of the desorption branch is due to hindered desorption, indicating slit-shaped pores.[46] As measured by BET (Brunauer-Emmet-Teller) method, the surface area was 550 cm^2 per cm^2 HNC. Thus the roughness factor of HNC was 550, much larger than that of NiO-TiO_2 nanotubes (38) with similar thickness and indicating higher specific surface area.[36] As shown from the BJH (Barrett-Joyner-Halenda) plot in Figure 3b, the HNC has a narrow pore size distribution around 4 nm. Such small pores might be generated during the removal of physically absorbed water or intercalated water molecules between $Ni(OH)_2$ layers.[47] The presence of high density small pores is favorable for electrolyte penetration, allows reaction species to quickly access the electrode and contributes to high capacitance.

To investigate the formation mechanism of the hierarchical structure of HNC, the transients of anodization parameters are measured and shown in Figure S1 (Supporting Information). Potential oscillation was found in the galvanostatic stage under the fine controlled processing condition. Oscillatory current or potential often resulted in modulated surface morphology.[48,49] There are two possible reasons for such oscillations. One is the cyclic growth and detachment of anodic oxides,[49] and the other is the limited diffusion of electrolyte ions.[48] In this study, the sequential growth and detachment of the HNC was not observed during the whole voltage oscillation stage. Thus the first mechanism did not seem to be applicable here. To see whether the voltage oscillation was caused by the second mechanism, vigorous electrolyte stirring was on and off during the anodization. Little influence of stirring on the potential oscillation was found (**Figure 4**a). Therefore, the oscillatory behavior of voltage was neither the result of limited electrolyte diffusion.

It was interesting to note that if galvanostatic mode was applied without initial potentiostatic holding at 0.7 V, there was no occurrence of such potential oscillation (Figure 4b).

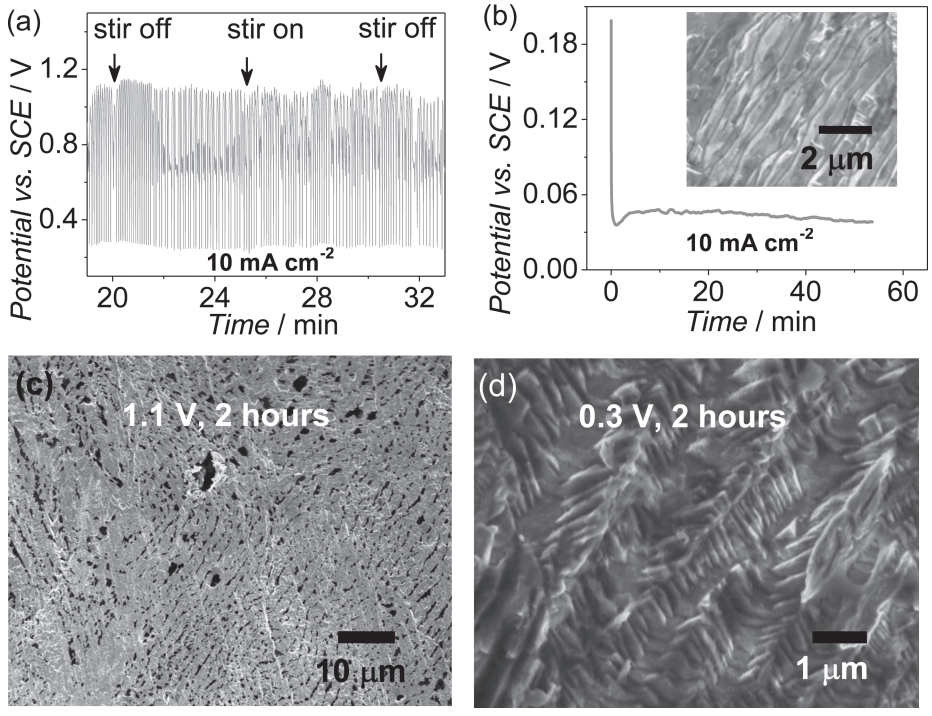

Figure 4. a) Potential-time transient showing the influence of electrolyte stirring on the potential oscillation. b) Potential-time transient for nickel anodized without initial potentiostatic holding at 0.7 V, inset shows the surface morphology of resulting anodic material. c,d) SEM images of nickel after being anodized at 1.1 and 0.3 V, respectively, for 2 h.

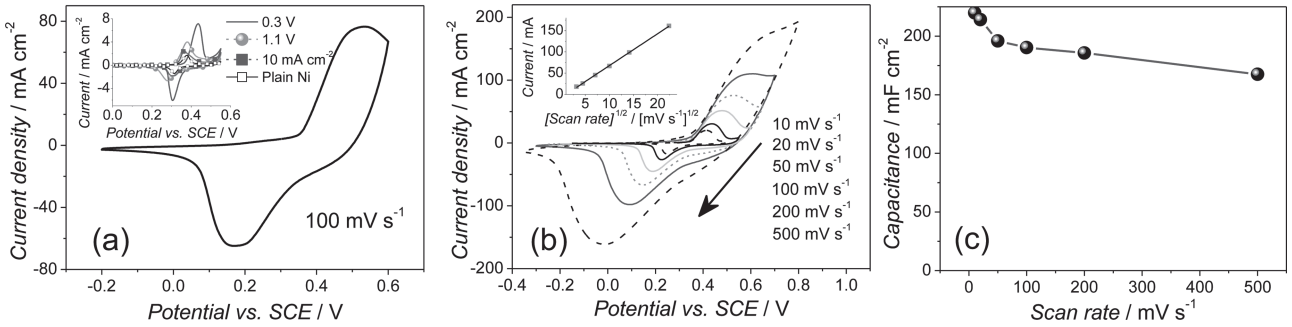

Figure 5. a) CV curve of HNC at 100 mV s^{-1}. Inset: CV curves of plain nickel, nickel after galvanostatic holding at 10 mA cm^{-2} and the samples after potentiostatic holding at 0.3 and 1.1 V, respectively. b) CV curves of HNC at different scan rates from 10 to 500 mV s^{-1}. Inset: linear relationship between cathodic peak current and square root of scan rate. c) The variation of scan rates with specific capacitance. CV solution: 1 M NaOH.

Consequently, hierarchical nanostructure was not observed. It was later found that oscillation happened only if the galvanostatic mode was applied when potential was over the passivation value (≈0.42 V as in Supporting Information Figure S1a). For example, no voltage oscillation was observed if the galvanostatic stage was applied after potentiostatic holding at 0.4 V, while the oscillation was observed if galvanostatic stage was applied after holding at 0.5 V. It is speculated that steady dissolution of nickel cannot be maintained if the anodization potential was higher than the passivation value. During subsequent galvanostatic holding, to meet the requirement of constant current density, nickel is automatically switched between activation (0.3 V) and over-passivation states (1.1 V). As a result, modulated (hierarchical) nanostructure is formed by a combination of severe localized dissolution and overall macro etching. To support above hypothesis, potentiostatic anodization was carried out for 2 h and the relevant SEM images are shown in Figure 4c,d. For the sample anodized at 1.1 V, severe dissolution of nickel happened and a lot of gas bubbles were generated. Many microsized etched holes were produced. For the sample anodized at 0.3 V, fishbone-like nanostructure was observed with the bone-width around 100 nm. Anyway, further work is still needed and in progress to understand the detailed mechanism of the potential oscillation. Whether such anodization tuning strategy is applicable to other non-valve metals (Co, Cu, etc.) to produce modulated structure remains to be investigated. It is worth noting that potential oscillation also occurred when CsCl in the electrolyte was replaced by other chlorides such as KCl or NaCl. However, HNC produced using CsCl shows the best electrochemical performance.

2.2. Electrochemical Properties

As indicated by SEM and BET results, HNC with high specific surface area and porous structure may be promising in versatile areas such as energy storage, catalysis and sensors. To demonstrate the application potential of HNC, its performance was evaluated as a supercapacitor electrode. Because HNC exhibited good mechanical adhesion and electrical connection to the current collector (Ni substrate), the addition of binder and conducting agent is unnecessary. Both the weight and volume of the electrode are expected to be reduced and the electrode preparation process is greatly simplified. The CV (cyclic voltammetry) curve of HNC is shown in **Figure 5**a. A pair of large redox peaks can be clearly identified, indicating that HNC was already electrochemical active in the as-grown state. By contrast, NiO-TiO_2 nanotubes developed elsewhere were not active in the as anodized state and a heat treatment was necessary to activate the material.[36] The color change was obvious for HNC during CV scan. When the sample was anodically polarized, it immediately turned dark while this color was completely bleached off during reverse scan. Such reversible color change corresponded to the reactions of Ni(II) ↔ Ni(III).[50] In the inset of Figure 5a, similar redox peaks were observed for plain nickel and the anodic samples without hierarchical nanostructure (corresponding SEM images shown in Figure 4b–d). However, the corresponding current densities were much reduced and the relevant color change was negligible, indicating much less active material involved in above reaction. The significantly lower current density of plain Ni confirmed the major contribution to high CV current in Figure 5a was due to HNC. The faradic reaction kinetics is represented by redox peak separation, with small separation indicating fast kinetics. Self-ordered nanoporous NiO/NiF_2 composite was fabricated by anodization of nickel in NH_4F containing solution.[37] Although the resulting material showed good electrochromic performance, the redox peak separation was very high (>0.7 V) at 100 mV s^{-1}. The much reduced peak separation of our HNC (0.34 V) indicates greatly enhanced reaction kinetics, which is important for electrode application to achieve high rate capability.

CV curves of HNC at different scan rates are shown in Figure 5b. The symmetric characteristic of the reaction peaks demonstrated the good reversibility of HNC,[3] which was also indicated by the high and stable coulombic efficiency (≈99%) in the galvanostatic charge/discharge test (Supporting Information Figure S2). The linear relationship between cathodic peak current and the square root of scan rates indicated that the reaction was diffusion controlled. The areal capacitance was calculated from the integration of CV curves

$$C = \frac{\int I(V)\mathrm{d}V}{\Delta V v} \quad (1)$$

where I is the current density, v is the scan rate and ΔV is the potential window. At the scan rate of 500 mV s^{-1}, HNC demonstrated significantly better performance (167 mF cm^{-2},

70 times higher) than NiO-TiO_2 nanotube arrays (2.3 mF cm^{-2}) with similar thickness.[36] The areal capacitance of HNC was also higher than other nickel-based electrodes with thicker active material layer.[15,51–53] The specific capacitance decreased gradually with increasing scan rate (Figure 5c), which is due to decreasing utilization of active material caused by limited diffusion/migration of ions. As the result of fast reaction kinetics, the capacitance reduction is very small for HNC. Even when the scan rate was increased to 50 times (from 10 mV s^{-1} to 500 mV s^{-1}), the capacitance was only reduced by 24% from 220 to 167 mF cm^{-2}. Such rate capability of HNC was fascinating when compared with many other nickel-based electrodes reported very recently, such as $Ni(OH)_2$/graphene electrode (70% capacitance reduction for 50 times rate increase),[3] NiO nanosheet (72% capacitance reduction for 8 times rate increase),[39] nanoporous NiO (56% reduction for 10 times increase),[38] vertically aligned NiO-CoO nanosheet (60% reduction for 10 times increase),[54] nanoball-like mesoporous α-$Ni(OH)_2$ (32% reduction for 10 times increase),[55] and hierarchical b-$Ni(OH)_2$ nanoflakes (59% reduction for 10 times increase).[56] The significantly enhanced reaction kinetics is attributed to the improved mass transportation and excellent electron conduction within HNC, which is evident from the structural and morphological characterization as shown above.

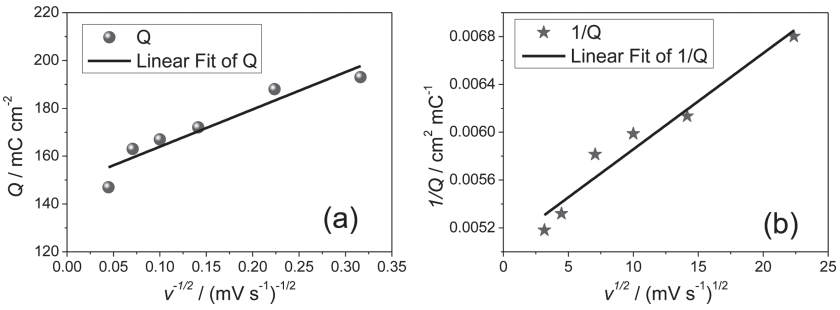

Figure 6. Variation of the voltametric charge Q with respect to scan rate ν: a) Q vs. $\nu^{-1/2}$ and b) $1/Q$ vs. $\nu^{1/2}$.

To understand why HNC could store/deliver charge with fast kinetics, we employed the analysis introduced by Trasatti et al.[57] The total charge storage (Q_T) can be divided into inner charge (Q_i) and outer charge (Q_O). Q_O is related to the charge stored at the surface, while Q_i depends on the diffusion within the electrode and corresponds to the less accessible region. Electrodes presenting a large ratio of Q_O over Q_T could exhibit a high rate capability. The different charges (Q_O, Q_i and Q_T) are estimated from the relationship of voltammetry charge Q with scan rate ν:

$$Q = \frac{1}{\nu}\int I(V)\mathrm{d}V \qquad (2)$$

Q_O was obtained from an extrapolation of Q to $\nu = \infty$ (**Figure 6**a). From the plot of $1/Q$ vs. $\nu^{1/2}$ (Figure 6b), the total charge Q_T was derived from an extrapolation of Q to $\nu = 0$. Q_i was then calculated as $Q_T - Q_O$. The charges of HNC were found to be 198.0, 49.6 and 148.4 mC cm^{-2} for Q_T, Q_i and Q_o, respectively. The high ratio of Q_o/Q_T (0.75) indicates a large proportion of the charges located at easily accessible sites and a high utilization of active material.[57,58]

The excellent electrochemical performance of HNC was further confirmed by EIS (electrochemical impedance spectroscopy) measurement as shown in **Figure 7**. The Nyquist impedance plot was composed of a straight line in low frequencies (0.01 to 125 Hz) and a depressed semicircle in high frequencies (601 to 100 kHz). ESR (equivalent series resistance) was determined by the interception of high frequency arc with the real axis, and was found to be 1.02 Ω cm^{-2}. ESR comes from various types of resistance such as the electrolyte resistance, contact resistance between active material and current collector, and the resistance of electrode matrix.[59] Low ESR value proved the high conductivity of HNC and the excellent electric contact between HNC and Ni substrate. The semicircle was associated with electrode surface properties and corresponded to the charge transfer resistance, which is a well-known limiting factor for rate capability of supercapacitor. The charge transfer resistance in this study was only 0.84 Ω cm^{-2}, much smaller than those reported elsewhere.[38,54,60] Such small resistance of HNC is highly desirable for the power density improvement. Another important parameter for electrode material, knee frequency, can also be obtained from the EIS spectra. The knee frequency is defined as the frequency at which the lowest imaginary impedance is found or the frequency at which the impedance starts to be dominated by its imaginary part.[61] Electrode material with high knee frequency is expected to deliver high powers for supercapacitors.[61] From the inset of Figure 7, the knee frequency was found to be around 125 Hz and implied enhanced reaction kinetics, since normally the knee frequency is less than 10 Hz for pseudocapacitors developed previously.[60–64]

Cycle life is also a key factor to be considered for supercapacitor electrode. Because supercapacitors are required to deliver power within a very short time, cycling with fast scan rate is

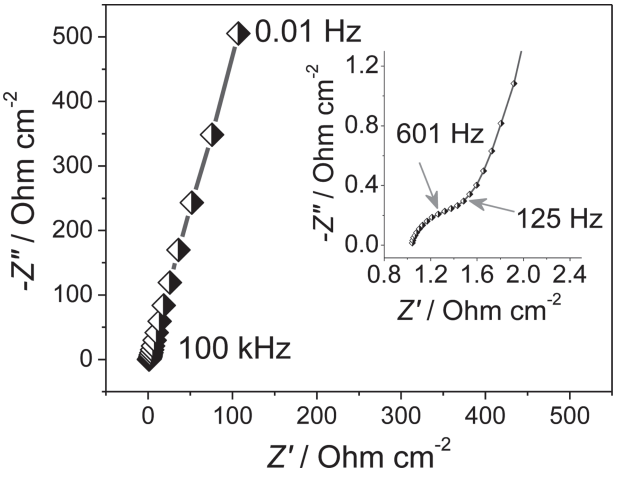

Figure 7. EIS spectra of HNC measured at 0.25 V (vs. SCE) with frequency ranged from 0.01 Hz to 100 kHz in 1 M NaOH. An enlargement at the high frequency region is shown in the inset.

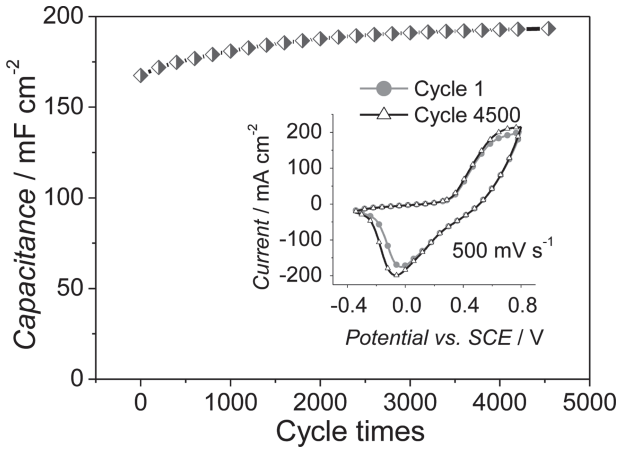

Figure 8. Cyclability test of HNC at 500 mV s^{-1} in 1 M NaOH, with inset showing the CV for cycle 1 and cycle 4500.

more desirable and represents the service performance of electrode material.[65] Thus cycling stability test was carried out for HNC using CV scan at 500 mV s^{-1} and the result is shown in **Figure 8**. Generally, capacitance loss is observed for electrode that utilizes insertion processes after long term test.[13,16,53,66,67] However, the electrode fabricated here demonstrates excellent cycle life, with the capacitance slowly increased during the test and reached 193 mF cm^{-2} after 4500 cycles. As shown in the inset, the last CV cycle almost overlapped with the first one, suggesting an extraordinary stability of HNC which was attributed to the following two factors: 1) the large free space in the 3D interconnecting nanoflakes architecture, where the volume change during redox reaction can be well accommodated; 2) the strong adhesion between HNC and the conducting substrate (HNC remained intact even after 30 min ultrasonication), which minimizes the detachment of active materials. The gradual increase of capacitance was also observed for $Ni(OH)_2$/graphene electrode[3] and NiO-TiO_2 nanotubes,[36] and can be ascribed to the improvement of electrode surface wetting by the electrolyte during extended cycling.[3] The morphology of HNC after 4500 cycles is shown in Supporting Information Figure S3. It is clear that the hierarchical and open channeled structure was still well maintained.

3. Conclusions

In summary, hierarchical nickel compound (HNC) was prepared as supercapacitor electrode by a fine controlled one-step and low cost electrochemical process without the need for hard/soft template. HNC exhibited good mechanical adhesion and electrical connection to the current collector, which makes the addition of binder and conducting agent unnecessary and facilitates the electrode fabrication process. Moreover, HNC demonstrated a 3D interconnecting structure with evenly distributed nanoscale open channels, providing large electrochemical active area and small charge transfer resistance. As a result of above advantages, HNC meets the requirements on high capacity, superior rate capability and long cycle life for energy storage applications. HNC performs much better than many supercapacitor electrodes reported previously. The performance of HNC is expected to be further improved by increasing the anodic film thickness, which can be achieved by suppressing the oxide dissolution speed in the electrolyte as in the case of Ti anodization.[20,68] Such investigation is going on in our group. Furthermore, due to the unique properties of HNC (good conductivity, structural stability, high porosity, etc.), HNC might also be promising for other functional applications such as catalysts, sensors and Li-ion batteries.

4. Experimental Section

Materials Preparation: All chemicals were of reagent grade and used as received. Nickel foils (0.2 mm thickness, 99.6% purity, Yirun Pte. Ltd., China) were degreased ultrasonically in acetone, isopropanol and ethanol for 10 min, respectively, followed by rinsing with de-ionized water and drying in hot air. Anodization of nickel was carried out by an electrochemical workstation (SP-150, Bio-Logic SAS, France) in unstirred aqueous solution containing H_2SO_4 (0.15 M) and CsCl (0.0375 M), with platinum as the counter electrode and saturated calomel electrode (SCE) as the reference. The anodization voltage was firstly ramped from open circuit potential to 0.7 V with a speed of 10 mV s^{-1}, followed by a potentiostatic holding at 0.7 V for 1 min, after which a constant current density of 10 mA cm^{-2} was applied for 200 min. After anodization, the sample was washed thoroughly with de-ionized water, followed by drying in hot air.

Characterization: SEM (LEO 1530 VP) and XRD (Rigaku D/max IIIA, Cu Kα) were used to characterize the morphology and crystalline structure. XPS (Kratos AXis Ultra DLD) was performed to study the chemical state. The binding energies of XPS signals have been corrected by assuming C 1s peak at 284.6 eV. Surface area was determined by the BET (Brunauer-Emmet-Teller) method using N_2 adsorption/desorption in Nova 4200. Pore size distribution was obtained by BJH (Barrett-Joyner-Halenda) method. Since the adhesion of HNC to Ni substrate was so strong that even after sonication in de-ionized water for 30 min, there was still no detachment of HNC. Therefore the N_2 adsorption/desorption was carried out using the as-anodized sample with the Ni substrate, and the data shown in Figure 3 was calculated per geometric area of HNC. The deduced pore size distribution and roughness factor (the ratio of real surface area over geometric surface area) were reasonably correct since the gas adsorbed by the Ni substrate is negligible. Electrochemical characterizations such as cyclic voltammetry (CV), galvanostatic charge/discharge and electrochemical impedance spectroscopy (EIS) were carried out by SP-150 in NaOH solution (1 M) with a standard three-electrode configuration.

Supporting Information

Supporting Information is available from the Wiley Online Library or from the author.

Acknowledgements

This work was supported by the Research Grants Council of the Hong Kong Special Administrative Region, China (Project: PolyU5187/09E), the Hong Kong Polytechnic University (Project Nos. A-PL16 and 5-ZG91), the Guangdong science and technology department under grant number of 2012A090300013, and the Fundamental Research Funds for the Central Universities (Project: 2012ZZ0011).

Received: November 21, 2012
Revised: December 31, 2012
Published online: February 19, 2013

[1] A. Bandara, J. Kubota, K. Onda, A. Wada, S. S. Kano, K. Domen, C. Hirose, *J. Phys. Chem. B* **1998**, *102*, 5951.
[2] Z. Tang, C. H. Tang, H. Gong, *Adv. Funct. Mater.* **2012**, *22*, 1272.
[3] J. Yan, Z. J. Fan, W. Sun, G. Q. Ning, T. Wei, Q. Zhang, R. F. Zhang, L. J. Zhi, F. Wei, *Adv. Funct. Mater.* **2012**, *22*, 2632.
[4] X. Xia, J. Tu, Y. Zhang, X. Wang, C. Gu, X.-b. Zhao, H. J. Fan, *ACS Nano* **2012**, *6*, 5531.
[5] L. Tao, J. Zai, K. Wang, Y. Wan, H. Zhang, C. Yu, Y. Xiao, X. Qian, *RSC Adv.* **2012**, *2*, 3410.
[6] L. Ji, Z. Lin, M. Alcoutlabi, X. Zhang, *Energy Environ. Sci.* **2011**, *4*, 2682.
[7] H. Huang, J. Tian, W. K. Zhang, Y. P. Gan, X. Y. Tao, X. H. Xia, J. P. Tu, *Electrochim. Acta* **2011**, *56*, 4281.
[8] Y. Ding, Y. Wang, L. C. Zhang, H. Zhang, Y. Lei, *J. Mater. Chem.* **2012**, *22*, 980.
[9] Y. G. Wang, Y. Y. Xia, *Electrochim. Acta* **2006**, *51*, 3223.
[10] M. Q. Wu, J. H. Gao, S. R. Zhang, A. Chen, *J. Porous Mater.* **2006**, *13*, 407.
[11] W. Xing, F. Li, Z. F. Yan, G. Q. Lu, *J. Power Sources* **2004**, *134*, 324.
[12] J. W. Lee, J. M. Ko, J.-D. Kim, *J. Phys. Chem. C* **2011**, *115*, 19445.
[13] Y. F. Yuan, X. H. Xia, J. B. Wu, J. L. Yang, Y. B. Chen, S. Y. Guo, *Electrochim. Acta* **2011**, *56*, 2627.
[14] S. H. Lee, C. E. Tracy, J. R. Pitts, *Electrochem. Solid State Lett.* **2004**, *7*, A299.
[15] Y. B. Xie, C. J. Huang, L. M. Zhou, Y. Liu, H. T. Huang, *Compos. Sci. Technol.* **2009**, *69*, 2108.
[16] G. W. Yang, C. L. Xu, H. L. Li, *Chem. Commun.* **2008**, 6537.
[17] P. Simon, Y. Gogotsi, *Nat. Mater.* **2008**, *7*, 845.
[18] H. Masuda, F. Hasegwa, S. Ono, *J. Electrochem. Soc.* **1997**, *144*, L127.
[19] D. Gong, C. A. Grimes, O. K. Varghese, W. Hu, R. S. Singh, Z. Chen, E. C. Dickey, *J. Mater. Res.* **2001**, *16*, 3331.
[20] J. M. Macak, H. Tsuchiya, L. Taveira, S. Aldabergerova, P. Schmuki, *Angew. Chem., Int. Ed.* **2005**, *44*, 7463.
[21] G. Zhang, H. Huang, Y. Zhang, H. L. W. Chan, L. Zhou, *Electrochem. Commun.* **2007**, *9*, 2854.
[22] G. K. Mor, O. K. Varghese, M. Paulose, C. A. Grimes, *Adv. Funct. Mater.* **2005**, *15*, 1291.
[23] L.-N. Wang, J.-L. Luo, *Electrochem. Commun.* **2010**, *12*, 1559.
[24] X. J. Feng, T. J. LaTempa, J. I. Basham, G. K. Mor, O. K. Varghese, C. A. Grimes, *Nano Lett.* **2010**, *10*, 948.
[25] K. Xie, J. Li, Y. Lai, W. Lu, Z. a. Zhang, Y. Liu, L. Zhou, H. Huang, *Electrochem. Commun.* **2011**, *13*, 657.
[26] J. E. Yoo, J. Choi, *Electrochim. Acta* **2010**, *55*, 5142.
[27] K. Zhu, N. R. Neale, A. Miedaner, A. J. Frank, *Nano Lett.* **2007**, *7*, 69.
[28] C. T. Yip, M. Guo, H. T. Huang, L. M. Zhou, Y. Wang, C. J. Huang, *Nanoscale* **2012**, *4*, 448.
[29] C. T. Yip, H. T. Huang, L. M. Zhou, K. Y. Xie, Y. Wang, T. H. Feng, J. S. Li, W. Y. Tam, *Adv. Mater.* **2011**, *23*, 5624.
[30] A. Ghicov, S. P. Alba, J. M. Macak, P. Schmuki, *Small* **2008**, *4*, 1063.
[31] G. K. Mor, M. A. Carvalho, O. K. Varghese, M. V. Pishko, C. A. Grimes, *J. Mater. Res.* **2004**, *19*, 628.
[32] G. G. Zhang, H. T. Huang, Y. S. Liu, L. M. Zhou, *Appl. Catal., B* **2009**, *90*, 262.
[33] G. Zhang, H. Huang, W. Li, F. Yu, H. Wu, L. Zhou, *Electrochim. Acta* **2012**, *81*, 117.
[34] K. Xie, J. Li, Y. Lai, Z. a. Zhang, Y. Liu, G. Zhang, H. Huang, *Nanoscale* **2011**, *3*, 2202.
[35] G. Zhang, C. Huang, L. Zhou, L. Ye, W. Li, H. Huang, *Nanoscale* **2011**, *3*, 4174.
[36] J. H. Kim, K. Zhu, Y. F. Yan, C. L. Perkins, A. J. Frank, *Nano Lett.* **2010**, *10*, 4099, and its correction, *Nano Lett.* **2011**, *11*, 5098.
[37] N. K. Shrestha, M. Yang, P. Schmuki, *Electrochem. Solid-State Lett.* **2010**, *13*, C21.
[38] K. Liang, X. Z. Tang, W. C. Hu, *J. Mater. Chem.* **2012**, *22*, 11062.
[39] X. Sun, G. K. Wang, J. Y. Hwang, J. Lian, *J. Mater. Chem.* **2011**, *21*, 16581.
[40] M. A. Kiani, M. F. Mousavi, S. Ghasemi, *J. Power Sources* **2010**, *195*, 5794.
[41] P. Oliva, J. Leonardi, J. F. Laurent, C. Delmas, J. J. Braconnier, M. Figlarz, F. Fievet, A. d. Guibert, *J. Power Sources* **1982**, *8*, 229.
[42] P. Jeevanandam, Y. Koltypin, A. Gedanken, *Nano Lett.* **2001**, *1*, 263.
[43] A. F. Carley, S. D. Jackson, J. N. O'Shea, M. W. Roberts, *Surf. Sci.* **1999**, *440*, L868.
[44] H. Jiang, T. Zhao, C. Li, J. Ma, *J. Mater. Chem.* **2011**, *21*, 3818.
[45] B. Sasi, K. G. Gopchandran, *Nanotechnology* **2007**, *18*, 115613.
[46] Z. K. Wang, J. M. Heising, A. Clearfield, *J. Am. Chem. Soc.* **2003**, *125*, 10375.
[47] J. W. Lee, T. Ahn, J. H. Kim, J. M. Ko, J.-D. Kim, *Electrochim. Acta* **2011**, *56*, 4849.
[48] W. Lee, J. C. Kim, U. Gosele, *Adv. Funct. Mater.* **2010**, *20*, 21.
[49] L. V. Taveira, J. M. Macak, K. Sirotna, L. F. P. Dick, P. Schmuki, *J. Electrochem. Soc.* **2006**, *153*, B137.
[50] M. S. Kim, T. S. Hwang, K. B. Kim, *J. Electrochem. Soc.* **1997**, *144*, 1537.
[51] J. H. Kim, S. H. Kang, K. Zhu, J. Y. Kim, N. R. Neale, A. J. Frank, *Chem. Commun.* **2011**, *47*, 5214.
[52] M.-S. Wu, Y.-A. Huang, J.-J. Jow, W.-D. Yang, C.-Y. Hsieh, H.-M. Tsai, *Int. J. Hydrogen Energy* **2008**, *33*, 2921.
[53] H. Wang, Y. Wang, X. Wang, *Electrochem. Commun.* **2012**, *18*, 92.
[54] X. Lu, X. Huang, S. Xie, T. Zhai, C. Wang, P. Zhang, M. Yu, W. Li, C. Liang, Y. Tong, *J. Mater. Chem.* **2012**, *22*, 13357.
[55] X. Q. Tian, C. M. Cheng, L. Qian, B. Z. Zheng, H. Y. Yuan, S. P. Xie, D. Xiao, M. M. F. Choi, *J. Mater. Chem.* **2012**, *22*, 8029.
[56] J. Yan, W. Sun, T. Wei, Q. Zhang, Z. Fan, F. Wei, *J. Mater. Chem.* **2012**, *22*, 11494.
[57] S. Ardizzone, G. Fregonara, S. Trasatti, *Electrochim. Acta* **1990**, *35*, 263.
[58] Z. Chen, V. Augustyn, X. Jia, Q. Xiao, B. Dunn, Y. Lu, *ACS Nano* **2012**, *6*, 4319.
[59] L. L. Zhang, X. S. Zhao, *Chem. Soc. Rev.* **2009**, *38*, 2520.
[60] B. R. Tao, J. A. Zhang, F. J. Miao, S. C. Hui, L. J. Wan, *Electrochim. Acta* **2010**, *55*, 5258.
[61] T. Y. Wei, C. H. Chen, K. H. Chang, S. Y. Lu, C. C. Hu, *Chem. Mater.* **2009**, *21*, 3228.
[62] Y. F. Ke, D. S. Tsai, Y. S. Huang, *J. Mater. Chem.* **2005**, *15*, 2122.
[63] F. Tao, Y. Q. Zhao, G. Q. Zhang, H. L. Li, *Electrochem. Commun.* **2007**, *9*, 1282.
[64] Y.-g. Wang, Y.-y. Xia, *Electrochim. Acta* **2006**, *51*, 3223.
[65] X. Wang, Y. Wang, C. Zhao, Y. Zhao, B. Yan, W. Zheng, *New J. Chem.* **2012**, *36*, 1902.
[66] G. Yu, L. Hu, N. Liu, H. Wang, M. Vosgueritchian, Y. Yang, Y. Cui, Z. Bao, *Nano Lett.* **2011**, *11*, 4438.
[67] L. Su, L. Gong, J. Gao, *J. Power Sources* **2012**, *209*, 141.
[68] M. Paulose, K. Shankar, S. Yoriya, H. E. Prakasam, O. K. Varghese, G. K. Mor, T. A. Latempa, A. Fitzgerald, C. A. Grimes, *J. Phys. Chem. B* **2006**, *110*, 16179.